Applied Thermal Engineering 252 (2024) 123661

Contents lists available at ScienceDirect

Applied Thermal Engineering

journal homepage: www.elsevier.com/locate/apthermeng

Research Paper

Conjugate heat transfer analysis of helium–xenon gas mixture in tight rod bundles

Junren Hou [a,b], Yuan Zhou [b,*], Shanfang Huang [a,*]

[a] Department of Engineering Physics, Tsinghua University, Beijing 100084, China
[b] College of Physics, Sichuan University, Chengdu 610065, China

ARTICLE INFO

Keywords:
Helium-xenon gas mixture
Tight rod bundles
Conjugate heat transfer
Heat flux redistribution
Pitch-to-diameter ratio

ABSTRACT

Helium-xenon gas mixture (He-Xe) and tight rod bundles are widely used in gas-cooled space nuclear reactors. However, few studies have been conducted on the effects of pitch-to-diameter ratio (*P/D*) on thermal–hydraulic characteristics while considering conjugate heat transfer. This paper numerically investigated He-Xe heat transfer in a fuel-gas gap-cladding-coolant structure of tight rod bundles. The numerical model is validated using experimental data and the maximum error of wall temperature is less than 5 %. The results show that conjugate heat transfer significantly affects the heat transfer. The heat transfer coefficient without conjugate heat transfer is only 8.85 % of that with conjugate heat transfer in the quasi-triangular pipe. The decrease in *P/D* enhances the convective heat transfer and causes larger pressure drops. A new performance evaluation criterion (*PEC*) is presented considering the effects of heat transfer, pressure drop and volume. *PEC* first increases and then decreases with the increase in *P/D* and the best comprehensive performance occurs at $P/D = 1.113$. The analysis of the temperature difference in the viscous sublayer ($y^+ < 5$) shows that the decrease in *P/D* enhances the turbulent effect of He-Xe and reduces the thickness of the viscous sublayer, resulting in the heat transfer enhancement. This study contributes to the optimal design of advanced space reactors.

1. Introduction

Nuclear energy, with its high-power density, high reliability and strong adaptability, is the inevitable choice for mankind to explore deep space. Nuclear reactors utilizing helium-xenon gas mixture (He-Xe) as coolant have attracted much attention, because of their light weight, small size and sufficient energy supply[1,2]. The United States, for example, initiated the Project Prometheus in 2003[3,4], aiming to develop the first nuclear reactor-powered propulsion system for a spaceship. The designed reactor was cooled by He-Xe. Although the project was cancelled later, it offered a valuable reference for the design of gas-cooled reactors. Recently, some researchers have designed various megawatt-class space nuclear reactors cooled by He-Xe and performed neutron and thermal–hydraulic analysis[5–8]. In addition to its application in space reactors, He-Xe is also used in land-based nuclear reactors. In 2024, Guan et al. [9] carried out an optimization study on the mass and efficiency of He-Xe Brayton cycle for mobile, land-based nuclear microreactors.

Past research has shown that the molar mass of He-Xe is commonly chosen to be 40 g/mol [10] considering the heat transfer of coolant and the aerodynamic loading of impeller blades. However, He-Xe with a molar mass of 40 g/mol has a very low Prandtl number (*Pr*) of 0.23 [11]. Consequently, the heat transfer characteristics of He-Xe differ from common fluids, challenging the thermal–hydraulic design of nuclear reactors. Thus, the study of He-Xe heat transfer has aroused increasing attention recently. Table 1 summarizes the existing relevant studies.

To reveal the mechanism of He-Xe heat transfer, the convective heat transfer of He-Xe in circular tubes has been widely investigated. In 1988, Tayler et al. [12] experimentally investigated the heat transfer of He-Xe in tubes and evaluated the applicability of Petukhov- Popov, Kays and Dittus-Boelter correlations. The test section was an Inconel 600 circular tube with an inner diameter of 5.87 mm. Results indicate that the relations of Petukhov-Popov and of Kays perform best. Zhou et al. [13–15] studied the He-Xe turbulent heat transfer in circular tubes. They proposed a modified turbulent Prandtl number model for He-Xe. Based on the turbulent boundary layer theory and calculation results, a heat transfer correlation of He-Xe was presented. Qin et al. [16] experimentally investigated the flow and heat transfer of He-Xe in a vertical heating tube and the experimental Reynolds number (*Re*) was in the range of $4000 - 3 \times 10^4$. They proposed new correlations for predicting the global Nusselt number (*Nu*). Wang et al. [17] numerically studied

* Corresponding authors.
E-mail addresses: zhouyuan1911@126.com (Y. Zhou), sfhuang@mail.tsinghua.edu.cn (S. Huang).

https://doi.org/10.1016/j.applthermaleng.2024.123661
Received 6 February 2024; Received in revised form 14 May 2024; Accepted 10 June 2024
Available online 10 June 2024

Nomenclature

Latin symbols

A	cross-sectional area, m^2
c	correlation coefficient
C_0	blackbody radiation coefficient, $W/(m^2 \cdot K^4)$
c_p	specific heat at constant pressure, $J/(kg \cdot K)$
D	outside diameter of rod bundle, m
D_h	hydraulic diameter, m
E	total energy, J/kg
f	friction factor
G	mass flux, $kg/(m^2 \cdot s)$
h	heat transfer coefficient, $W/(m^2 \cdot K)$
k	turbulence kinetic energy, m^2/s^2
L	effective heating distance, m
m	mass flow rate, kg/s
M	molar mass, g/mol
Nu	Nusselt number
p	pressure, $kg/(m \cdot s^2)$
P	pitch between tight rod bundles, m
Pr	Prandtl number
q	heat flux, W/m^2
Q	volume source, W/m^3
Re	Reynolds number
T	temperature, K
u	velocity, m/s
u'	fluctuating velocity, m/s
V	volume, m^3
W	wet perimeter of the cross-section, m
y	distance form wall, m
y^+	dimensionless wall distance
P/D	pitch-to-diameter ratio

Greek symbols

δ	thickness, m
Δ	diffference
ϵ	emissivity
λ	thermal conductivity, $W/(m \cdot K)$
μ	dynamic viscosity, $kg/(m \cdot s)$
ρ	density, kg/m^3
τ	shear stress, $kg/(m \cdot s^2)$
θ	angle relative to the center of rod bundle
υ	kinematic viscosity, m^2/s

Subscripts

ave	average
b	bulk temperature
f	friction
fuel	fuel
i	inner surface of gas gap
in	inlet
norm	normalization
o	outer surface of gas gap
out	outlet
sub	viscous sublayer
t	turbulent
w	wall
eff	effective

Table 1
Summary of previous literature on the heat transfer of helium-xenon gas mixture.

Researcher	Time	Channel type	P/D	Thermal boundary condition	Method
Tayler et al.	1988[12]	Circular tube	–	–	Experimental
Vitovsky et al.	2015[20,21]	Circular tube	–	–	Experimental
	2016[19]	Triangular pipe			
	2017[28]				
Qin et al.	2022[16]	Circular tube	–	–	Experimental
Vitovsky	2022[22]	Quasi-triangular pipe	1.000	–	Experimental
Makarov et al.	2022[23]	Quasi-triangular pipe	1.000	Conjugate heat transfer	Experimental & numerical
Qin et al.	2020[24]	Tri-lobe pipe	unknown	Constant heat flux	Numerical
Zhou et al.	2020[15]	Circular tube	–	Constant heat flux	Numerical
	2021[6,13,14]				
Sun et al.	2022[25]	Quasi-triangular pipe	1.000	Constant heat flux	Numerical
Ning et al.	2023[26]	Tight rod bundles	1.092	Constant heat flux	Numerical
Wang et al.	2023[27]	Wire-wrapped rod bundles	unknown	Constant heat flux	Numerical
Wang et al.	2023[17]	Circular tube	–	Conjugate heat transfer	Numerical

the heat transfer characteristics of He-Xe in circular coolant channels with conjugate heat transfer. They analyzed the influence of power distribution on local Nusselt number and presented a correlation to predict local Nusselt number.

To better utilize He-Xe in nuclear reactors, much research has focused on its thermal–hydraulic characteristics in different geometries, especially for quasi-triangular channels (an extreme approximation of tight rod bundles). Vitovsky [18–21] conducted experimental studies on the He-Xe heat transfer with $Pr = 0.23$ in circular and triangular cross section channels and compared the heat transfer rules with known correlations. Results show that the heat transfer rates of triangular cross section channels were lower than those of circular channels due to the presence of stagnant region near slits. Vitovsky [22] also investigated the heat transfer of He-Xe in a heated quasi-triangular channel and proposed a method for calculating local heat transfer coefficients in unsteady flows. Makarov et al. [23] also experimentally and numerically studied the thermal–hydraulic characteristics of He-Xe in a quasi-triangular pipe. Qin et al. [24] numerically investigated the heat transfer characteristics of He-Xe in tri-lobe channels for constant heat flux boundary conditions. They found that the wall temperature at the tri-lobe channels slits was significantly higher than that at the concavities. Sun et al. [25] compared the heat transfer characteristics of He-Xe, CO_2 and Na in quasi-triangular channels for constant heat flux boundary conditions. They claimed that the thermal property of CO_2 is the best. Ning et al. [26] numerically investigated the flow and heat transfer characteristics of He-Xe in tight rod bundles. The pitch-to-diameter ratio (P/D) of rod bundles was 1.092 and the boundary conditions of rod bundles were constant heat flux. They analyzed the transition from laminar flow to turbulent flow of He-Xe. Additionally, Wang et al. [27] also investigated the thermal–hydraulic characteristics of He-Xe in wire-

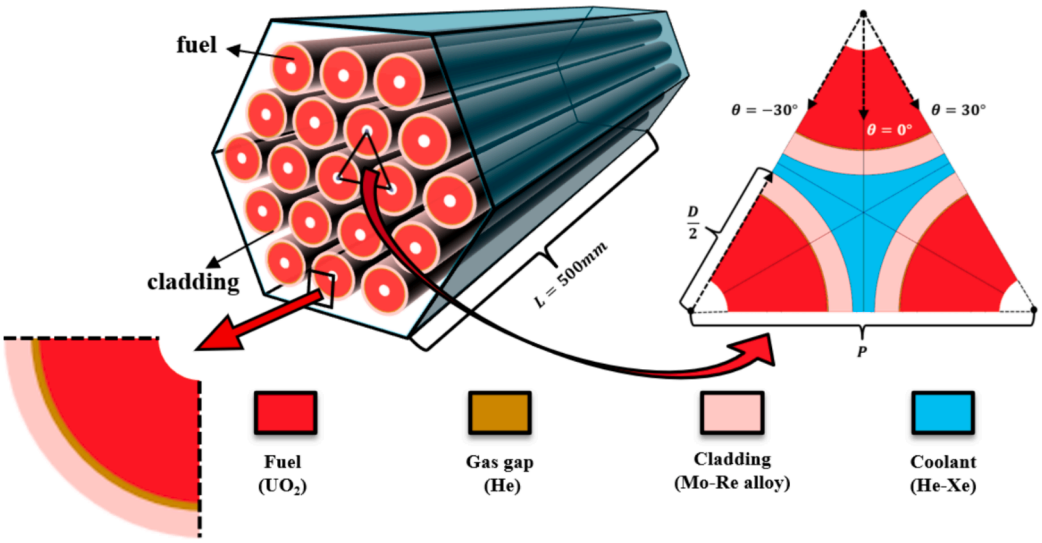

Fig. 1. Geometric diagram of tight rod bundles.

Table 2
Specific geometric parameters.

Parameters	Value
Fuel inner diameter	3 mm
Fuel outer diameter	11.2 mm
Gas gap thickness	0.05 mm
Cladding thickness	1 mm
Cladding outer diameter	13.3 mm
Effective heating distance	500 mm
Pitch	13.3 ~ 16.0 mm
Pitch-to-diameter ratio	1 ~ 1.20

wrapped rod bundles for constant heat flux.

Some progress has been made in the field of He-Xe convective heat transfer, but some research gaps remain. As the literature review above and Table 1 show that most studies applied constant heat flux boundary condition to the tight rod bundles. The thermal conduction of fuel, gas gap and cladding should be considered in the real case. This simplified boundary condition will result in error and affect the heat transfer rules of He-Xe. However, it is still unclear how much error this simplified boundary condition will introduce. Further research is urgently needed. Table 1 also shows that tight rod bundles are widely used in gas-cooled nuclear reactors. To make the reactors smaller, most of the literature has studied P/D in the range of 1 to 1.1 (much less than 1.33 for typical pressurized water reactors [29–31]). However, there is a dearth in research on the influence of P/D on the thermal–hydraulic characteristics of tight rod bundles.

The purpose of this study was to explore the effects of P/D on thermal–hydraulic characteristics considering conjugate heat transfer. This paper numerically investigated the convection heat transfer of He-Xe with a molar mass of 40 g/mol in tight rod bundles. The thermal conduction of fuel, gas gap and cladding is considered. Firstly, we compared the differences of convective heat transfer with and without conjugate heat transfer and found the heat flux redistribution in the cladding. Then, we analyzed the influence of P/D on the thermal–hydraulic characteristics of tight rod bundles with conjugate heat transfer. These characteristics included heat transfer, pressure drop and velocity field. Finally, we analyzed the heat transfer mechanisms in tight rod bundles for various P/D. This study improves the understanding of the He-Xe convection heat transfer and contributes to the optimal design of advanced space reactors.

2. Numerical method

2.1. Governing equations and discretization schemes

The convective heat transfer of He-Xe in tight rod bundles was analyzed using computational fluid dynamics. The governing equations were solved using Fluent software package. The advection terms were discretized using the second order upwind method. Pressure and velocity were coupled using SIMPLE method. When the maximum temperature no longer varies with the iteration and residuals have decreased 4 orders of magnitude, the calculation is considered to be converged. The governing equations to be solved are as follows (steady state problem, ignoring the time term).

Solid domain:

$$\frac{\partial}{\partial x_i}\left(\lambda\frac{\partial T}{\partial x_i}\right)+Q=0 \tag{1}$$

Fluid domain:

$$\frac{\partial}{\partial x_i}(\rho u_i)=0 \tag{2}$$

$$\frac{\partial}{\partial x_j}\left(\rho u_i u_j\right)=-\frac{\partial p}{\partial x_i}+\frac{\partial}{\partial x_i}\left[\mu\left(\frac{\partial u_i}{\partial x_j}+\frac{\partial u_j}{\partial x_i}-\frac{2}{3}\delta_{ij}\frac{\partial u_l}{\partial x_l}\right)-\rho\overline{u_i'u_j'}\right] \tag{3}$$

$$\frac{\partial}{\partial x_i}\left(u_i(\rho E+p)\right)=\frac{\partial}{\partial x_i}\left(\lambda_{\text{eff}}\frac{\partial T}{\partial x_i}\right) \tag{4}$$

where the turbulent thermal conductivity λ_t is calculated by the turbulence model [32]. $-\rho\overline{u_i'u_j'}$ is the Reynolds stress term and represents the stress caused by turbulent fluctuations. According to the Boussinesq hypothesis, Reynolds stress item can be expressed as:

$$-\rho\overline{u_i'u_j'}=-p_t\delta_{i,j}+\mu_t\left(\frac{\partial u_i}{\partial x_j}+\frac{\partial u_j}{\partial x_i}\right) \tag{5}$$

where $p_t=2\rho k/3$ is the pressure caused by turbulent fluctuations, k is the turbulence kinetic energy and μ_t is the turbulence viscosity calculated by turbulence model. In the present paper, the Reynolds stress term and turbulent thermal conductivity were calculated using the SST $k-\omega$ turbulence model that has been widely used to investigate the convection heat transfer of He-Xe [13,17,24,33]. More information of SST $k-\omega$ turbulence model can be found in Menter's work [34].

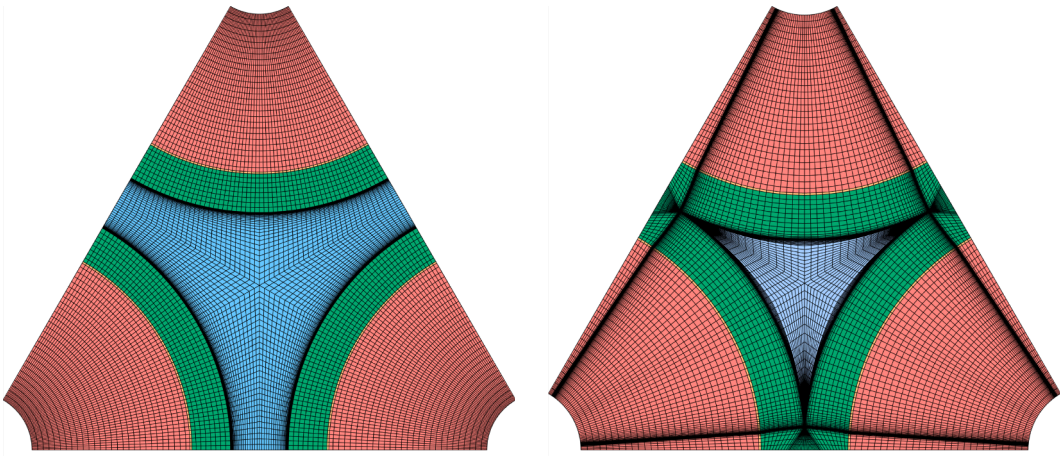

(a) Meshing method for $P/D > 1$. (b) Meshing method for $P/D = 1$.

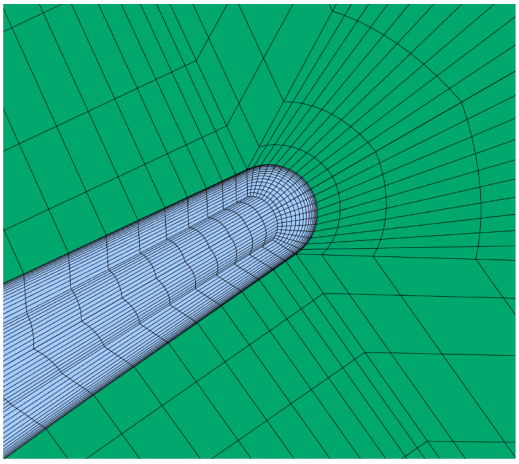

(c) Meshing method at slits for $P/D = 1$.

Fig. 2. Structured mesh diagram.

Table 3
Thermal properties of helium-xenon gas mixture.

Properties	Value	Unit
ρ	Ideal gas	kg/m^3
c_p	519.6	J/(kg·K)
λ	$-1.067\times10^{-8}T^2+1.298\times10^{-4}T+0.03985$	W/(m·K)
μ	$-4.887\times10^{-12}T^2+5.563\times10^{-8}T+1.511\times10^{-5}$	kg/(m·s)
M	40	g/mol

2.2. Geometry and Meshing

Fig. 1 illustrates the geometry of the present simulation and Table 2 summarizes the corresponding geometric parameters. The main parameters are based on the gas-cooled space nuclear reactor designed by Tao et al. [8]. This study investigates the conjugate heat transfer of fuel, gas gap and cladding. The gas gap is filled with helium at 2 MPa. The convection of helium is neglected because it is very weak for a thickness of 0.05 mm. The effect of helium gap on heat transfer is discussed in the Appendix section. To reduce the computational cost, only 1/12 of the rod bundles are simulated due to the geometric symmetry. The mirror and rotation features are used in Tecplot for visual enhancement. As the fluid enters, the boundary layer will gradually develop from 0 at the entrance to fill the entire channel. Thus, the heat transfer at the entrance is usually overestimated. At the same time, due to the turbulent pulsation, there may be a backflow phenomenon at the outlet, which will affect the heat transfer near the outlet. Therefore, unheated sections of 100 mm ($> 20D_h$) are placed at the entrance zone and exit zone to eliminate the entrance effect and the backflow phenomenon in outlet [13,26,33].

A fine structured mesh is generated using ICEM, as shown in Fig. 2. The mesh is refined near the cladding outer wall with a first element height of 0.003 mm. The dimensionless wall distance is always less than 1. The dimensionless wall distance y^+ is defined as Eq. (6). When $P/D > 1$, the mesh generation method in Fig. 2(a) is applied. When $P/D = 1$, the line contact between the rod bundles degrades the mesh quality. Following our previous work [35], rounded slits with a radius of 0.02 mm are used to simplify the geometry and generate a high-quality structured mesh at the slits, as shown in Fig. 2(b,c). The structured mesh used in this paper facilitates the analysis of the heat transfer mechanism of He-Xe.

$$y^+ = y\frac{\sqrt{\tau_w/\rho}}{\upsilon} \tag{6}$$

where y is the first element height, τ_w is the wall shear stress and υ is the kinematic viscosity.

2.3. Physical properties and boundary conditions

In this study, UO_2 is used as the fuel material and its thermal conductivity is calculated by Eq. (7) [36]. The physical properties of helium at 2 MPa are obtained from the NIST Standard Reference Databases

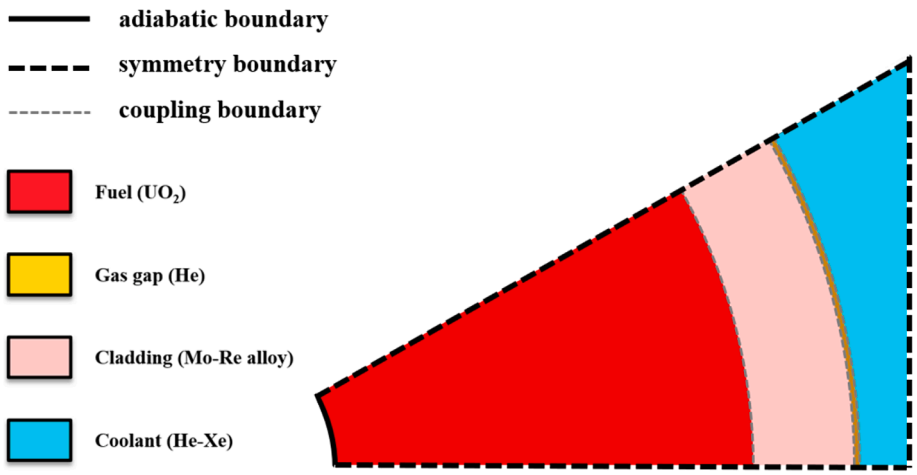

Fig. 3. Boundary condition diagram where each line represents a surface parallel to flow direction.

Table 4
Meshing settings.

	Element size of cross section (mm)	Number of elements	Max temperature (K)	Number of axial elements
Mesh 1	0.10	565,880	1869.4	140
Mesh 2	0.15	267,960	1870.0	140
Mesh 3	0.20	180,612	1871.9	140
Mesh 4	0.30	98,962	1875.3	140
Mesh 5	0.15	401,940	1870.2	210

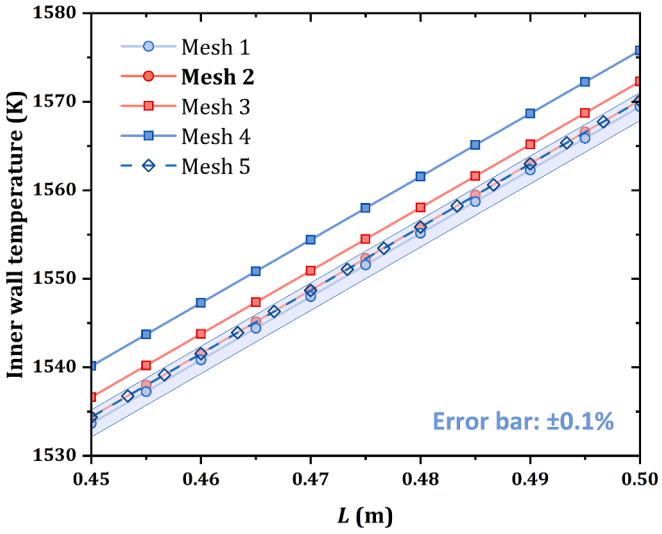

Fig. 4. Results of inner wall temperature for different mesh.

Table 5
Experimental conditions for model validation.

	T_{in} (K)	P (Pa)	q (W/m^2)	M (g/mol)	G (kg/(m^2·s))
Case 1	297.5	488,149	45,081	40	149.3
Case 2	299.3	991,466	159,071	40	267.5
Case 3	295.8	471,502	43,637	83.8	350.6
Case 4	303.0	806,581	296,622	14.5	139.7

[37]. Mo-50 Re alloy is used as the cladding material and its physical properties are derived from Lundberg's work [38]. Eq. (8) shows the polynomial fitting formula of the thermal conductivity. In 2006, Tournier et al. [11,39] reviewed the thermophysical properties of noble gases and their binary mixtures and developed semi-empirical correlations based on the Chapman-Enskog kinetic theory for dilute gases. The thermophysical properties of He-Xe in this study are computed by using their correlations. Table 3 presents the detailed settings of the He-Xe physical properties.

$$\lambda_{UO_2} = \frac{115.8}{(7.5408 + 17.629t + 3.6142t^2)} + 7410.5t^{-5/2}\exp\left(-\frac{16.35}{t}\right) \ \mathrm{W}/(\mathrm{m}\cdot\mathrm{K}) \tag{7}$$

with $t = T(\mathrm{K})/1000$.

$$\lambda_{Mo-Re} = -2.952 \times 10^{-6}T^2 + 0.02013T + 43.10 \ \ \mathrm{W}/(\mathrm{m}\cdot\mathrm{K}) \tag{8}$$

To avoid the inlet/outlet effect, unheated sections of 100 mm length are placed at the inlet and outlet. The fuel inner wall is an adiabatic boundary, the other outer boundaries parallel to the flow direction are symmetry boundaries and the inner boundaries parallel to the flow direction are coupling boundaries, as shown in Fig. 3. The inlet boundary condition is mass-flow-rate-inlet and the outlet boundary condition is pressure-outlet. A volume source term is applied to the fuel. The specific values of the boundary conditions are inlet temperature of 1134.4 K, outlet temperature of 1500 K and outlet pressure of 2 MPa. The Mach number corresponding to inlet velocity is less than 0.3 for all the calculated conditions in this paper. The volume source term of the fuel is calculated according to the mass flow rate and the calculation formula is given by:

$$Q = \frac{mc_p(T_{out} - T_{in})}{V_{fuel}} \tag{9}$$

2.4. Mesh independence verification and model validation

Five different sets of mesh were used for mesh independence verification and their specific settings are shown in Table 4. Mesh 1–4 varied the element sizes on the cross section and Mesh 2 and 5 divided different numbers of elements in the axial direction. Results in Fig. 4 shows that the results of Mesh 2 and 5 agree completely, indicating that 140 elements are sufficient in the axial direction. The difference between the results of Mesh 1 and 2 is less than 0.1 %, indicating that the mesh independence is verified. Finally, Mesh 2 is used.

In this study, the numerical model is validated by using the tube experiment of Tayler et al. [12]. Four groups of different experimental

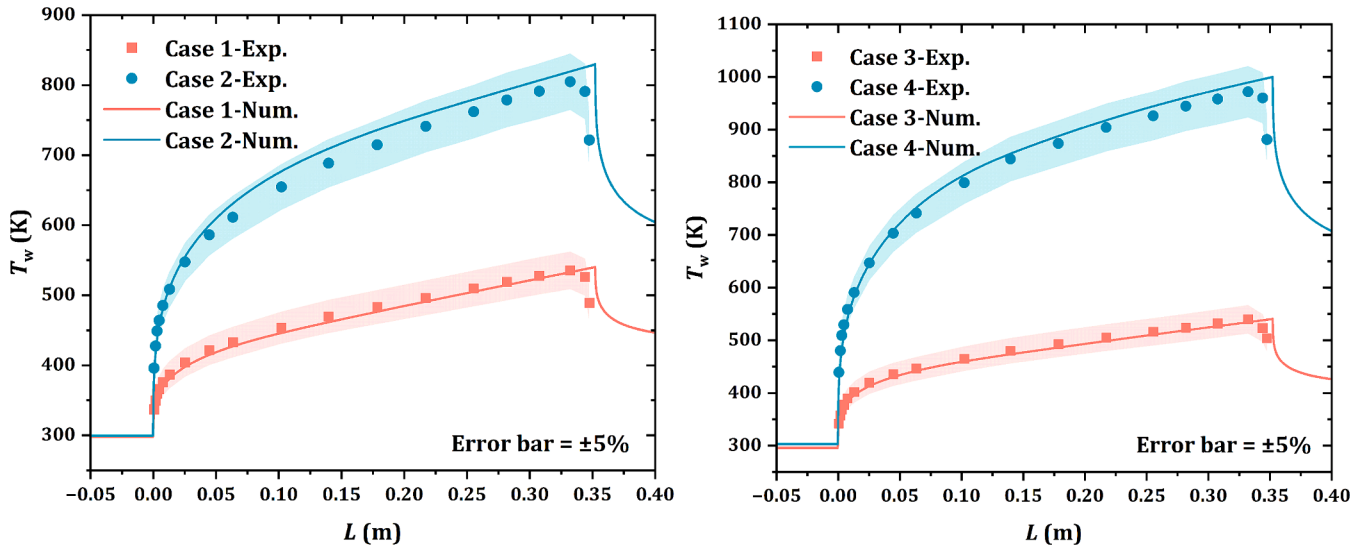

Fig. 5. Comparisons of numerical results and experimental data.

conditions are chosen to cover various pressure, heat flux and helium-xenon molar mass. The specific setting parameters are listed in Table 5. The geometry calculated was a circular tube with an inner diameter of 5.87 mm. Its effective heating distance is 60 diameters (352.2 mm). Unheated sections of 100 mm are also placed at the inlet and outlet to reduce the impact of inlet and outlet effects. Fig. 5 compares the numerical results with the experimental data. The relative errors of wall temperature are all below 5 %, confirming the correctness of the model.

3. Results and discussion

3.1. The effect of conjugate heat transfer on thermal–hydraulic characteristics of He-Xe

This section analyzed the effect of conjugate heat transfer on He-Xe convective heat transfer. Fig. 6(a) displays the outer wall temperature of cladding with and without conjugate heat transfer for $P/D = 1.113$ (unless otherwise stated, this paper analyzes the thermal–hydraulic characteristics at an effective heating distance of 400 mm). Due to the symmetry of the wall temperature, only the part of $\theta > 0^{\circ}$ was discussed. The results indicate that the temperature distribution on the cladding wall is relatively nonuniform when conjugate heat transfer is not considered. For the constant heat flux boundary condition, the wall temperature increases with the increase in θ and the temperature difference reaches 80 K. When θ approaches 0°, the wall temperature predicted with conjugate heat transfer is higher than that without conjugate heat transfer. When θ approaches 30°, the predicted wall temperature with conjugate heat transfer is lower than that without conjugate heat transfer. On average, the constant heat flux boundary overestimates the outer wall temperature of cladding. Fig. 6(b) demonstrates that conjugate heat transfer redistributes the wall heat flux distribution on the outer wall of the cladding. The heat flux becomes nonuniform and decreases with the increase in θ. This uneven distribution of heat flux raises the wall temperature near $\theta = 0^{\circ}$ and lowers the wall temperature near $\theta = 30^{\circ}$, which flattens the wall temperature distribution. Fig. 6(b) also reveals that the heat flux on the inner wall of the cladding is uniform, which implies that the redistribution of heat flux occurs in the cladding. This is due to the fact that the thermal conductivity of cladding is much higher than that of the fuel and helium. In the calculation, the average thermal conductivity of Mo-Re is 64.74 W/(m·K). The average thermal conductivity of UO_2 is 3.104 W/(m·K). The average thermal conductivity of helium is 0.444 W/(m·K).

Fig. 6(c) shows the outer wall temperature distribution of the cladding for a quasi-triangular channel ($P/D = 1$) at $Re = 7853$ (Re is calculated as Eq. (10)). The basic distribution trend agrees $P/D = 1.113$. However, when θ approaches 30°, the wall temperature reaches a peak of 3800 K, which is unrealistic. Due to the peak wall temperature, the average wall temperature is overestimated by about 600 K without conjugate heat transfer temperature. Fig. 6(d) shows the role of heat flux redistribution in flattening the outer wall temperature. The heat flux increases to three times the average heat flux for $\theta = 0^{\circ}$ and drops to 0 for $\theta > 20^{\circ}$.

$$Re = \frac{GD_h}{\mu_b} = \frac{4m}{\mu_b W} \tag{10}$$

where $D_h = 4A/W$ is the hydraulic diameter. Eq. (10) shows that since W and μ_b are constants in this study, Re corresponds to m one to one.

The heat flux vector in Fig. 7 illustrates the heat flux redistribution of the cladding. The results indicate that the velocity in the mainstream area is high and the wall temperature near the mainstream area is low, which results in heat transfer from both sides to the center. The smaller the P/D, the more heat is transferred to the vicinity of the mainstream. When $P/D = 1$, the heat flux vector near $\theta = 30^{\circ}$ is almost tangent to rod.

Fig. 8 compared the pressure drop and heat transfer difference with and without conjugate heat transfer. The results in Fig. 8(a) indicate that conjugate heat transfer has no effect on pressure drop. However, conjugate heat transfer have a strong effect on heat transfer. As shown in Fig. 8(b), the average wall temperature increases and the heat transfer coefficient decreases with the increase in P/D considering conjugate heat transfer. When conjugate heat transfer is not considered, the wall temperature first decreases and then increases with the increase in P/D and the threshold of P/D is 1.113. The heat transfer coefficient exhibits the opposite trend, first increasing and then decreasing with the increase in P/D, as shown in Fig. 8(c). The reason for this phenomenon is that when P/D approaches 1 there will be a temperature peak near $\theta = 30^{\circ}$ without conjugate heat transfer (see Fig. 6). With the increase of P/D, the peak phenomenon will weaken and the temperature will gradually decrease. When P/D is large enough, the peak phenomenon disappears and the heat transfer coefficient increases with the increase of P/D, as shown when conjugate heat transfer is considered. It's worth noting that the heat transfer coefficient without conjugate heat transfer is only 8.85 % of that with conjugate heat transfer in the quasi-triangular pipe. The analysis above in this paragraph implies that the wrong heat transfer rule is obtained without conjugate heat transfer as P/D approaches 1.

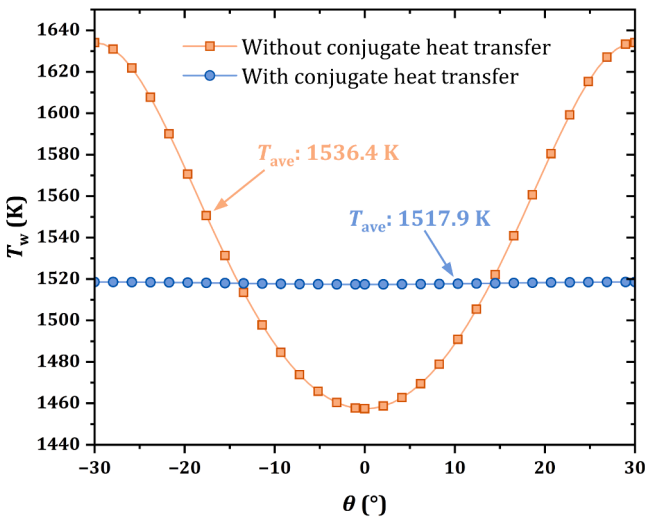

(a) Comparison of wall temperature for P/D=1.113.

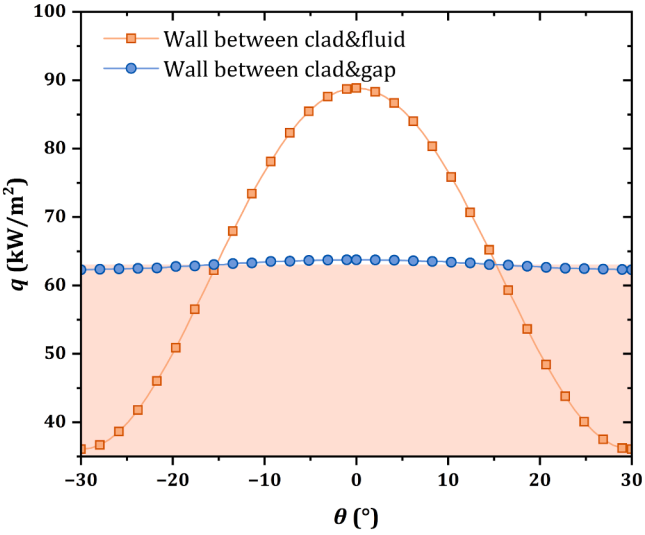

(b) Comparison of heat flux for P/D=1.113.

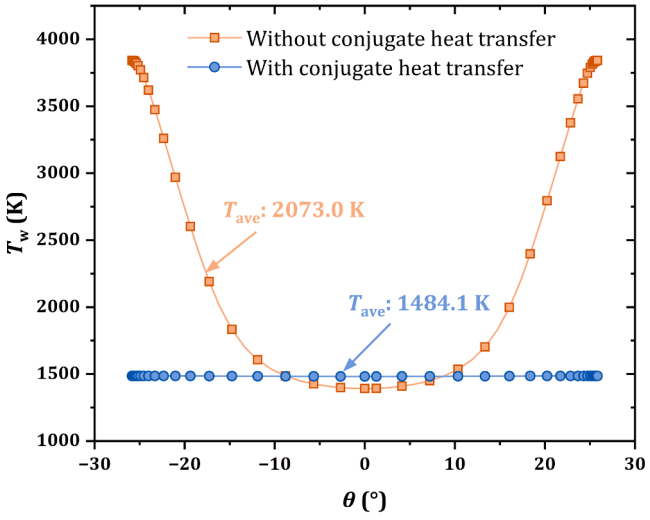

(c) Comparison of wall temperature for P/D=1.

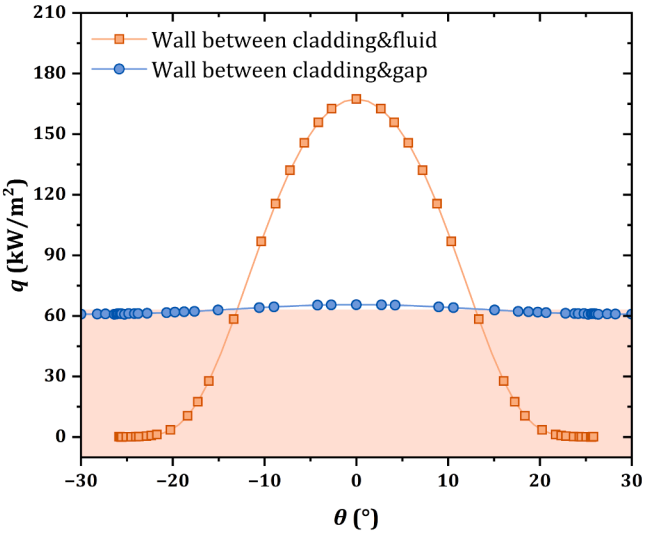

(d) Comparison of heat flux for P/D=1.

Fig. 6. Comparison of effects of conjugate heat transfer on wall temperature and heat flux for Re = 7853. The heat flux between the gas gap and the cladding is multiplied by a factor C = 11.3/13.3.

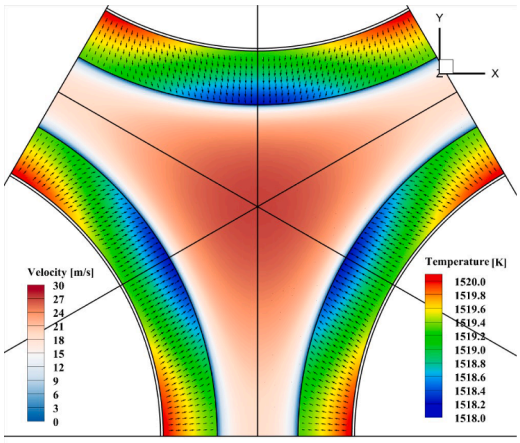

(a) P/D = 1.113

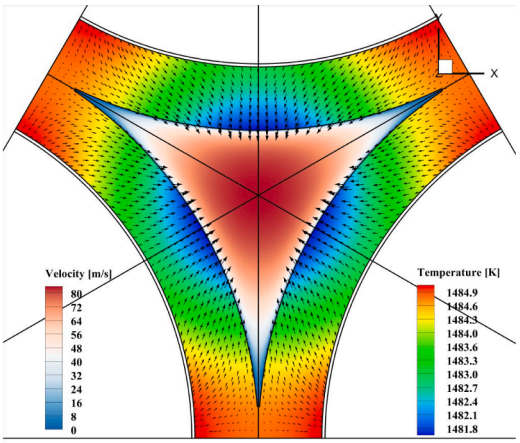

(a) P/D = 1

Fig. 7. The heat flux vector at cladding and coutours of temperature and velocity.

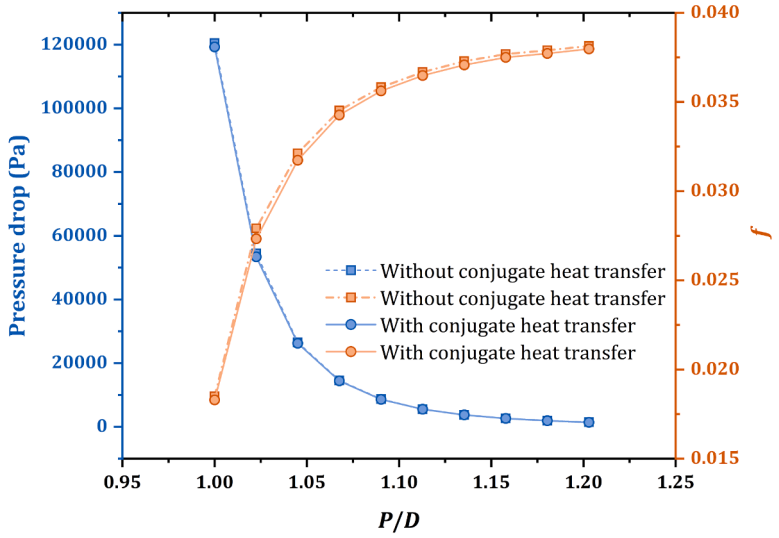

(a) Effect of P/D on pressure drop and friction factor.

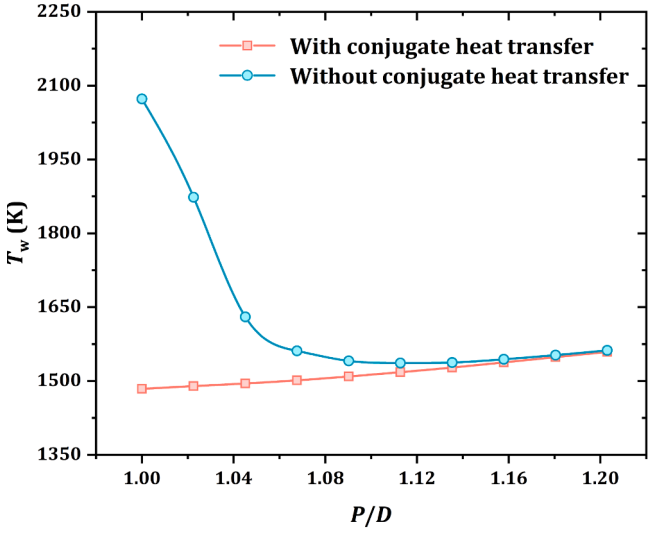

(b) Effect of P/D on wall temperature.

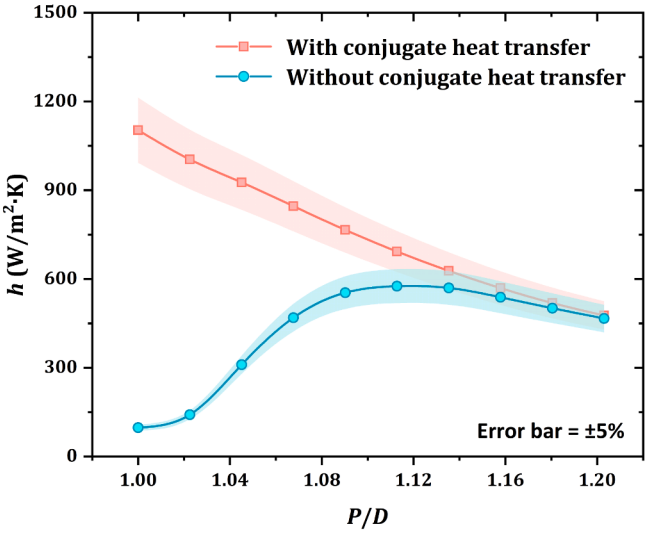

(c) Effect of P/D on heat transfer cofficient.

Fig. 8. Comparisons of results with and without conjugate heat transfer for $Re = 7853$. T_w is the average wall temperature at the effective heating length of 400 mm. h is calculated by $q/(T_w - T_b)$.

Therefore, it is essential to consider conjugate heat transfer in the numerical study of He-Xe heat transfer in tight rod bundles.

3.2. Thermal-hydraulic characteristics in dense rod bundles for various pitch-to-diameter ratios

3.2.1. Temperature field in dense rod bundles

Fig. 9 shows the temperature field in tight rod bundles. The results indicate that the fluid temperature at the slit is higher than that at the main flow region. The temperature gradient near the wall of $\theta = 0^{\circ}$ is larger than that of $\theta = 30^{\circ}$, leading to the higher wall heat flux as shown in Fig. 6. The comparison of the results for various P/D shows that the increase in P/D lowers the wall temperature and flattens the temperature distribution.

3.2.2. Velocity field in dense rod bundles

Result in Fig. 10 shows that He-Xe will accumulate toward the middle at the inlet, resulting in an increase in velocity at the main flow region and a decrease at the slit. Fig. 10 also indicates that the velocity gradually increases with the increasing of flow distance due to the thermal expansion of He-Xe. Fig. 11 illustrates the normalized velocity in the dense rod bundles. The results show that the increase in P/D increase the normalized velocity of the main flow region. This implies an increase in P/D causes more fluid to accumulate toward the middle. However, because the flow area at slits for $P/D = 1$ becomes smaller and less fluid accumulates towards the center, the normalized velocity of the main flow region for $P/D = 1$ shows a decrease compared to $P/D = 1.023$.

3.2.3. Heat transfer characteristics in dense rod bundles

Fig. 12 illustrates the variation of average wall temperature and heat transfer coefficient with Re for various P/D. The results show that the heat transfer coefficient increases with increasing Re. Because the volume source term applied to the fuel needs to be proportional to Re for the outlet temperature to be consistent, the wall temperature also increases with increasing Re. The results in Fig. 12 also demonstrate that the wall temperature increases with the increase in P/D and the heat transfer coefficient decreases with the increase in P/D at the same Re.

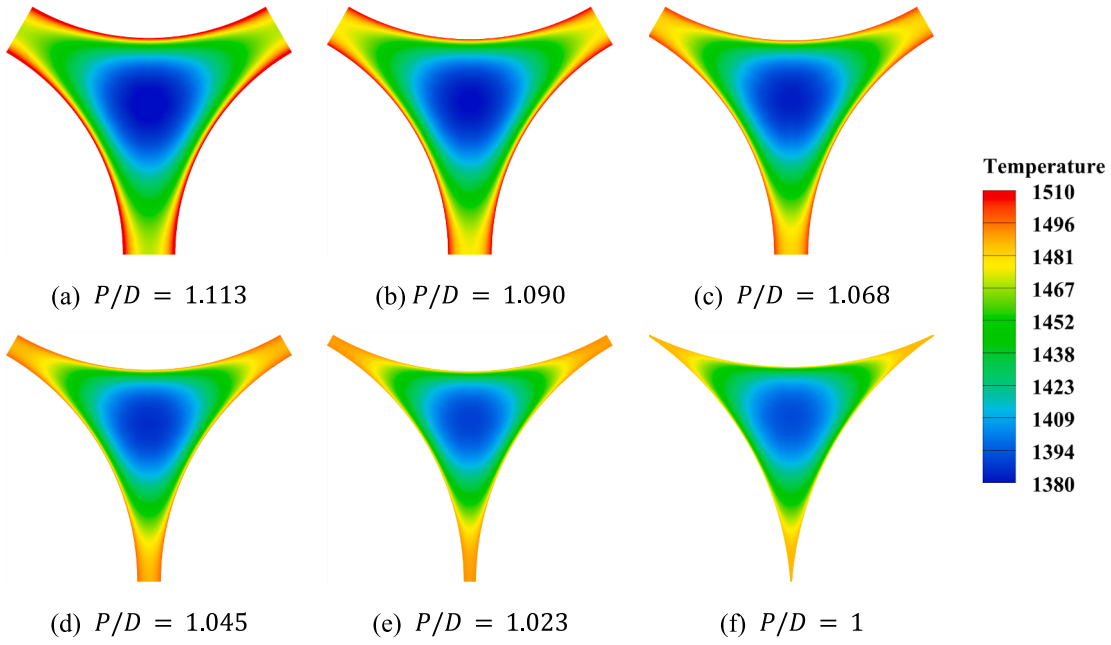

Fig. 9. Temperature contours at the effective heating distance of 400 mm for $Re = 7853$. The corresponding bulk temperature is 1426.9 K.

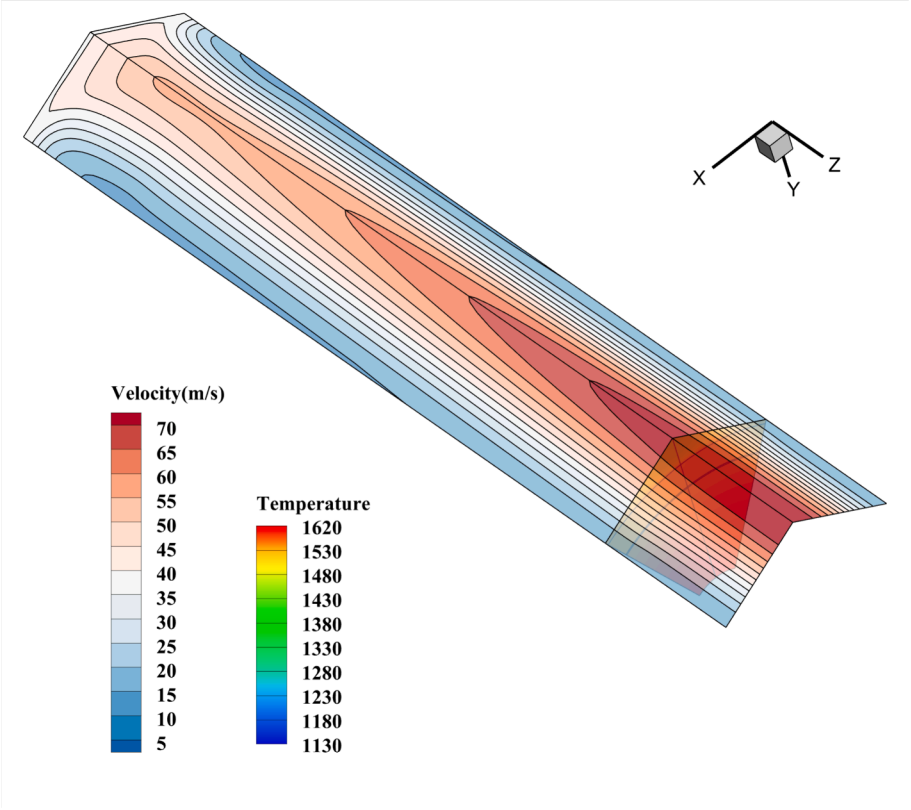

Fig. 10. Velocity contours at the middle vertical planes of the lines between rod bundle centers for $P/D = 1.023$. The temperature contour is at the effective heating distance of 400 mm.

This implies that the increase in P/D reduces the convective heat transfer of He-Xe. Section 3.3 analyzed the reason for this phenomenon.

Fig. 13 shows the variation of Nu with Re for various P/D, where Nu is defined as Eq. (11). The results indicate that Nu increases with the increase in Re and P/D. The reason that the trends of Nu and heat transfer coefficient with P/D are different is that D_h will increase with the increase of P/D and the effect of increasing D_h is greater than the effect of decreasing h. Fig. 13 also indicates that Dittus-Boelter [40] and Kays [41] correlations can not predict He-Xe heat transfer in tight rod bundles accurately. The average error increases as P/D decreases. The maximum error is more than 100 %. Dittus-Boelter correlation is expressed as Eq. (12). Kays correlation is expressed as Eq. (13). In this

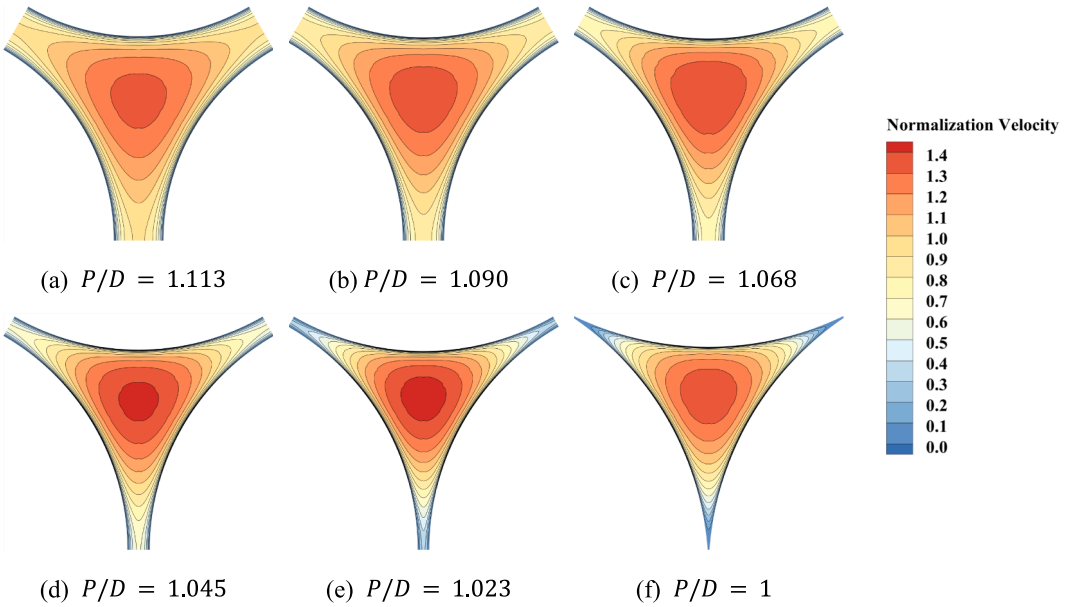

Fig. 11. Normalization velocity contours at the effective heating distance of 400 mm for $Re = 7853$. ($u_{norm} = u/u_{ave}$).

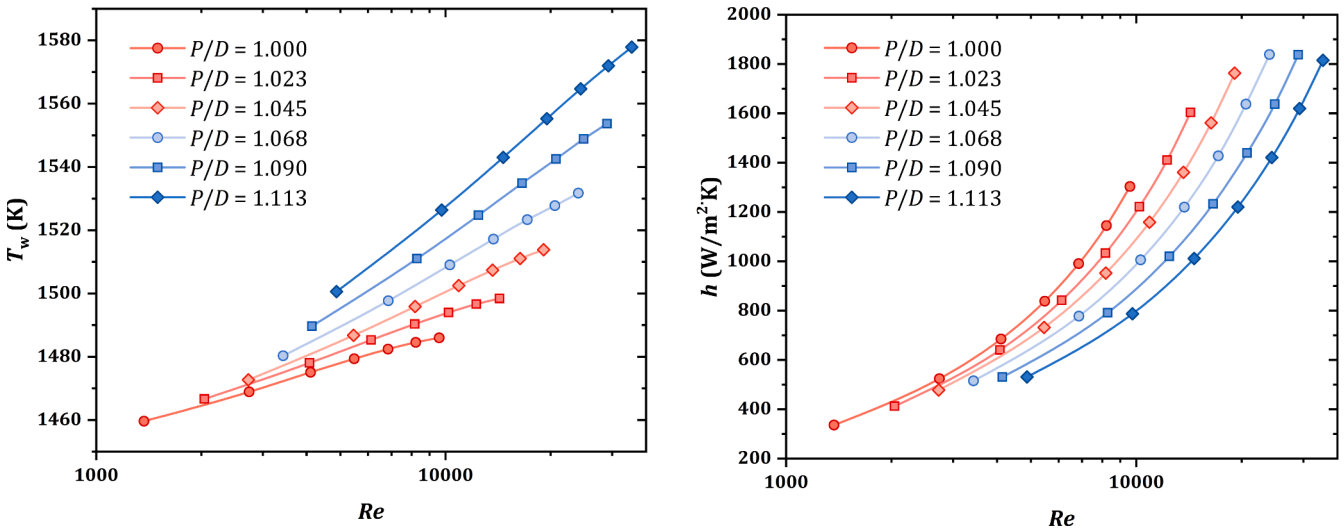

(a) Effect of P/D on average wall temperature. (b) Effect of P/D on heat transfer coefficient.

Fig. 12. Heat transfer characteristics in dense rod bundles for various P/D. T_w is the average wall temperature at the effective heating length of 400 mm. h is calculated by $q/(T_w - T_b)$.

study, the geometric shape factor of $(P/D - c_1)^{c_2}$ is introduced based on the common empirical correlation formula. The correlation coefficient was obtained by fitting the results of CFD. The error between the presented correlation and CFD is within 10 %, as shown in Fig. 14. Equation (14) shows the specific form of the correlation. The proposed correlation reflects the trend of Nu increasing with the increase of Re and P/D.

$$Nu = \frac{hD_h}{\lambda} \tag{11}$$

where h is the heat transfer coefficient, λ is the thermal conductivity for bulk temperature.

$$Nu = 0.023Re^{0.8}Pr^{0.4} \tag{12}$$

$$Nu = 0.022Re^{0.8}Pr^{0.6} \tag{13}$$

$$Nu = 0.0740Re^{0.6712}\left(\frac{P}{D} - 0.9917\right)^{0.2988} \tag{14}$$

3.2.4. Pressure drops characteristics in dense rod bundles

Fig. 15 illustrates the variation of the pressure drop and the friction factor with Re for various P/D. The friction factor is defined as Eq. (15). The results indicate that the pressure drop increases with the increase in Re and the friction factor decreases with the increase in Re. For the same Re, the pressure drops decrease with the increase in P/D, while f increases with the increase in P/D. This implies that the Reynolds number decreases with the decrease in P/D for the same pressure drops. Since $Q_{fuel} \propto m \propto Re$, the fuel power and mass flow rate will also decrease as P/D decreases. This means that the smaller the P/D, the smaller the power density of the rod bundle. Fig. 15(b) also indicates that Blasius correlation [42] can not predict the friction factor in tight rod bundles

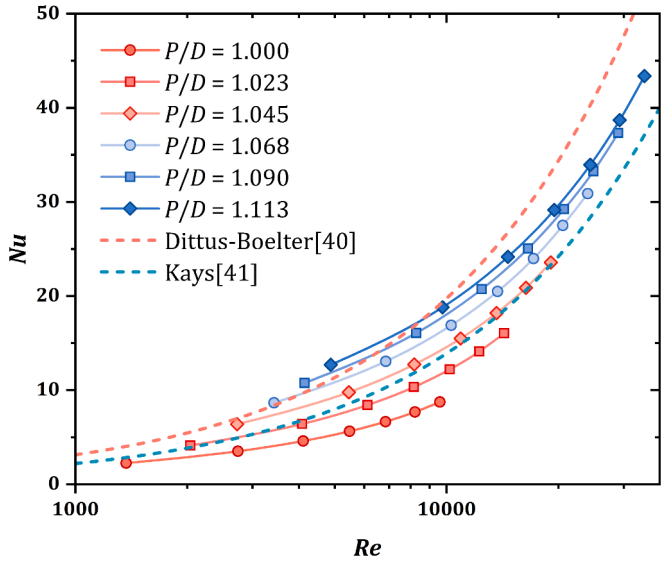

Fig. 13. Effect of P/D on Nu for various Re.

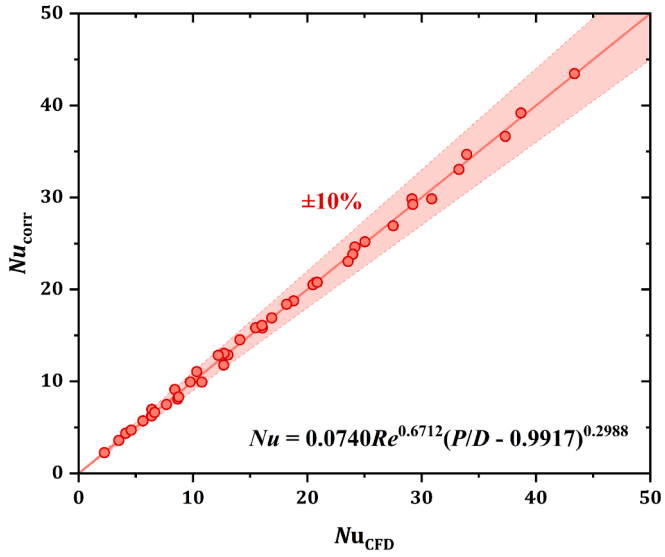

Fig. 14. Comparison between the results of the correlation and CFD.

accurately. The average error increases as P/D decreases. The maximum error is more than 100 %. Blasius correlation is expressed as Eq. (17). The geometric shape factor of $(P/D - c_1)^{c_2}$ is introduced to fit the friction factor. The error between the presented correlation and the CFD results is within 10 %, as shown in Fig. 16. Eq. (18) is the specific form of the correlation.

$$f = 2\frac{\Delta P_f D_h}{GLu_{ave}} \tag{15}$$

where L is the effective heating distance, u_{ave} is the average velocity, ΔP_f is the friction pressure drops.

$$\Delta P_f = P_{in} - P_{out} - \frac{G^2}{\overline{\rho}}\left[\frac{T_{out} - T_{in}}{\overline{T}} + \ln\frac{P_{in}}{P_{out}}\right] \tag{16}$$

where $\overline{\rho}$ and $\overline{T}$ represent the average density and temperature of the tube.

$$f = \frac{0.3164}{Re^{0.25}} \tag{17}$$

$$f = \frac{1.5914}{Re^{0.3694}}\left(\frac{P}{D} - 0.9967\right)^{0.1946} \tag{18}$$

3.2.5. The evaluation of comprehensive performance

Figure of merit (*FOM*) and performance evaluation criterion (*PEC*) were used to evaluate the comprehensive performance of heat transfer enhancement and larger pressure drop. *FOM* is widely used by many studies and defined in Eq. (19) [43–45]. Because f and Nu gradually flattened with the increase of P/D, as shown in Fig. 17, f and Nu at $P/D = 1.203$ are used as reference values. The result in Fig. 18 shows that the *FOM* decreases with the decrease in P/D indicating a decrease of the thermal–hydraulic comprehensive performance. However, *FOM* does not consider the effect of volume, which is an important parameter for the design of space reactors. The volume of the tight rod bundles is calculated from Eq. (20), which is proportional to the square of P/D. Therefore, this study proposes a new evaluation criterion *PEC* considering heat transfer, pressure drop and volume effects. *PEC* is defined in Eq. (21) as *FOM* divided by $(P/D)^2$. As shown in Fig. 18, *PEC* first increases and then decreases with the increase in P/D and the maximum value is at $P/D = 1.113$, indicating that the best comprehensive performance occurs at $P/D = 1.113$.

It is worth mentioning that the current optimal design of nuclear reactors is primarily a consideration of neutronic physics. The ultimate goal must surely be to design a reactor that combines neutronic and thermal–hydraulic considerations. The neutronic physics and thermal–hydraulic are generally analyzed separately in detail. Subsequently, simplified models are developed for coupled design based on in-depth knowledge. The work in this section can provide an optimal thermal–hydraulic point for the optimal design of rod bundles. It can contribute to the optimal design of advanced nuclear reactors. For example, in rod bundle design, we can consider the shorter distance from the thermal–hydraulic optimum as an optimization objective.

$$FOM = \frac{Nu/Nu_{ref}}{\left(f/f_{ref}\right)^{1/3}} \tag{19}$$

$$V = \frac{1}{2}P\cdot\frac{\sqrt{3}}{2}P\cdot L = \frac{\sqrt{3}}{4}P^2L = \frac{\sqrt{3}}{4}D^2L\left(\frac{P}{D}\right)^2 \tag{20}$$

$$PEC = \frac{FOM}{(P/D)^2} = \frac{Nu/Nu_{ref}}{\left(f/f_{ref}\right)^{1/3}(P/D)^2} \tag{21}$$

3.3. Heat transfer mechanism for various pitch-to-diameter ratios

This section analyzes the reason why the convective heat transfer of He-Xe increases as P/D decreases. Fig. 19 depicts the turbulent viscosity ratio profiles for various P/D. The turbulent viscosity ratio characterizes the magnitude of the role of turbulent fluctuation [46]. The results indicate that the turbulent viscosity ratio is larger in the main flow region than in the slits, which implies that turbulent fluctuation plays a dominant role in the main flow region. With decrease in P/D, cross sectional area decreases and hence for same mass flow rate, velocity will increase. Therefore, the turbulent viscosity ratio increases as P/D decreases (See Fig. 19), leading to the decrease in the thickness of viscous sublayer, as shown in Fig. 20. When P/D decreases from 1.113 to 1, the thickness of viscous sublayer at $\theta = 0^\circ$ decreases from 0.045 mm to 0.013 mm, with a decrease of 71 %. Because of the complete fit of rod bundles, the fluid velocity decreases to 0 m/s, resulting in an increase in

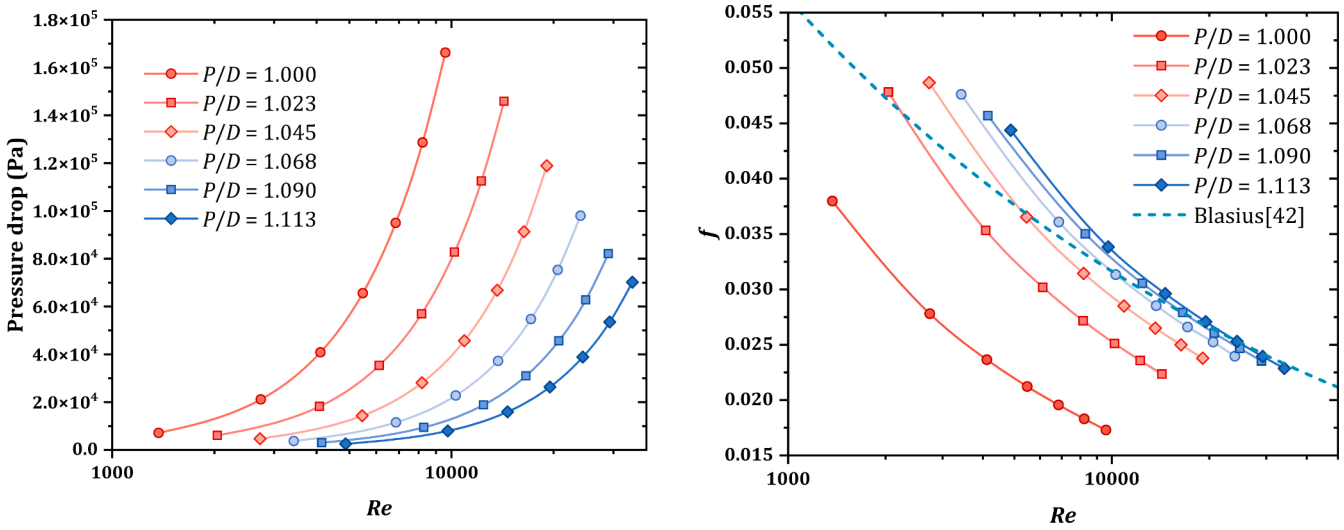

(a) Effect of P/D on pressure drop. (b) Effect of P/D on friction factor.

Fig. 15. Pressure drops characteristics in dense rod bundles for various P/D.

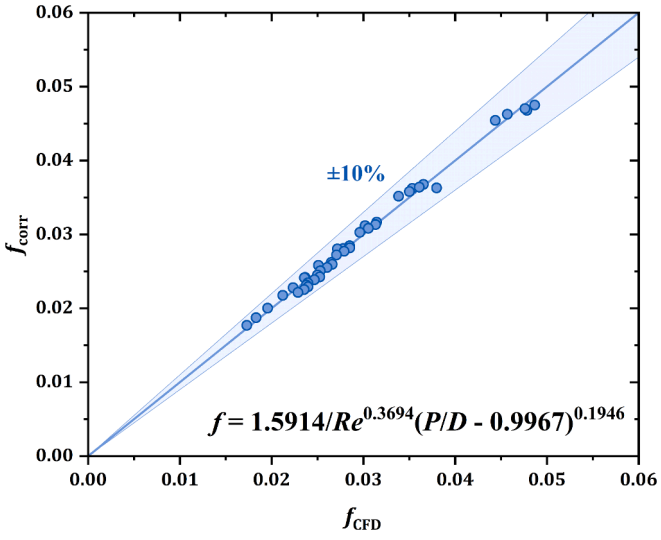

Fig. 16. Comparison between the results of the correlation and CFD.

the thickness of the viscous sublayer at $\theta = 30^{\circ}$ for $P/D = 1$. In this paper, the region with $y^{+}<5$ is considered as the viscous sublayer [47]. The definition of the thickness of viscous sublayer is given by Eq. (22).

$$\delta_{sub} = y|_{y^{+}=5} = \frac{5\upsilon}{\sqrt{\tau_w/\rho}} \tag{22}$$

The heat transfer rate of turbulent flow is significantly stronger than that of laminar flow. In the viscous sublayer region, heat transfer mainly relies on heat conduction. Therefore, reducing the thickness of the viscous sublayer enhances the heat transfer and reduces the wall temperature. The results in Fig. 21. show that the heat flux becomes more nonuniform as P/D decreases due to the heat conduction of cladding. When P/D decreases from 1.113 to 1, the heat flux at $\theta = 0^{\circ}$ doubles and the heat flux at $\theta = 30^{\circ}$ decreases from 36 kW/m^2 to 0. Since the wall temperature is determined by both the heat flux and the thickness of viscous sublayer, ΔT_{sub} is defined in Eq. (23) to evaluate their combined effect.

$$\Delta T_{sub} = q\frac{\delta_{sub}}{\lambda} \tag{23}$$

where q is the wall heat flux, δ_{sub} is the thickness of viscous sublayer and λ is the thermal conductivity. The physical meaning of δ_{sub}/λ is the thermal resistance of viscous sublayer. The physical meaning of ΔT_{sub} is the increase in wall temperature due to the viscous sublayer.

Fig. 22 illustrates the variation of ΔT_{sub} with P/D. The results show that ΔT_{sub} decreases as P/D decreases for $\theta = 0^{\circ}$ 30° and the two have a good linear relationship. The reasons for the enhanced He-Xe heat transfer with decreasing P/D are summarized as follows based on the analysis in this section. The decrease in P/D enhances the effect of turbulence and reduces the thickness of viscous sublayer, which is conducive to heat transfer. Although the heat flux redistribution will increase the wall heat flux at $\theta = 0^{\circ}$, the decrease in thermal resistance caused by the reduction in thickness of the viscous sublayer is greater. The net result is that a decrease in P/D enhances the turbulent heat transfer of He-Xe in tight rod bundles.

4. Conclusions

Although He-Xe convective heat transfer have been extensively investigated, few studies have been conducted on the effects of pitch-to-diameter ratio (P/D) on thermal–hydraulic characteristics for considering conjugate heat transfer. This paper investigated the conjugate heat transfer of He-Xe in tight rod bundles with a molar mass of 40 g/mol. Fine structured meshes were generated for numerical simulations. The SST $k-\omega$ turbulence model, which has been experimentally validated, was selected for the analysis. The main conclusions are as follows:

- Conjugate heat transfer has a significant impact on the heat transfer characteristics and is essential to be considered. The heat transfer

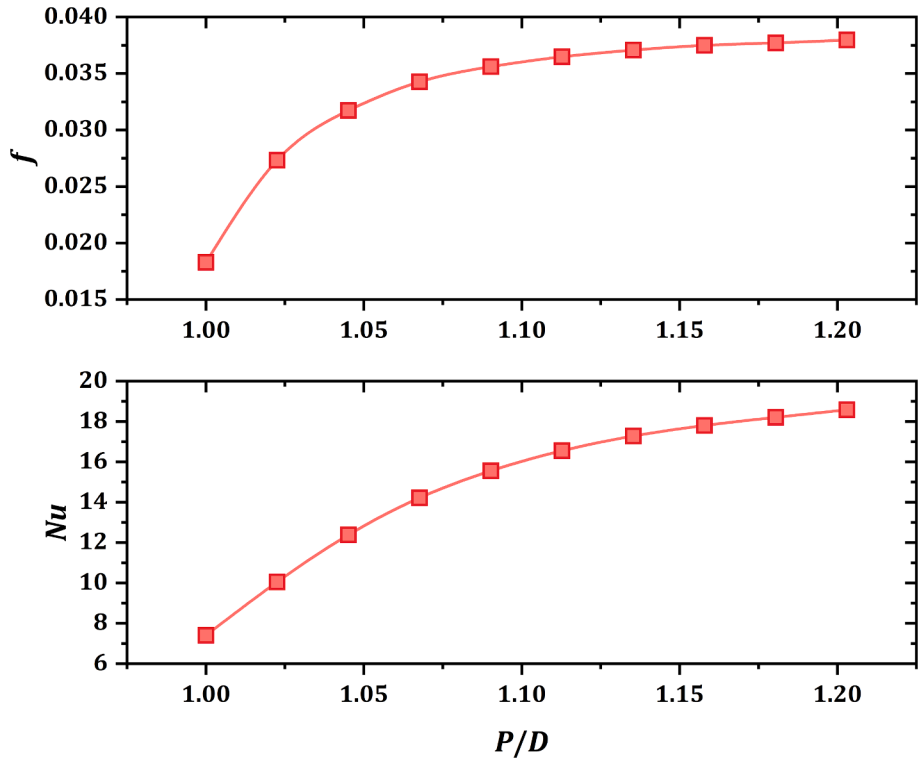

Fig. 17. Friction factor and Nusselt number for various P/D for $Re = 7853$.

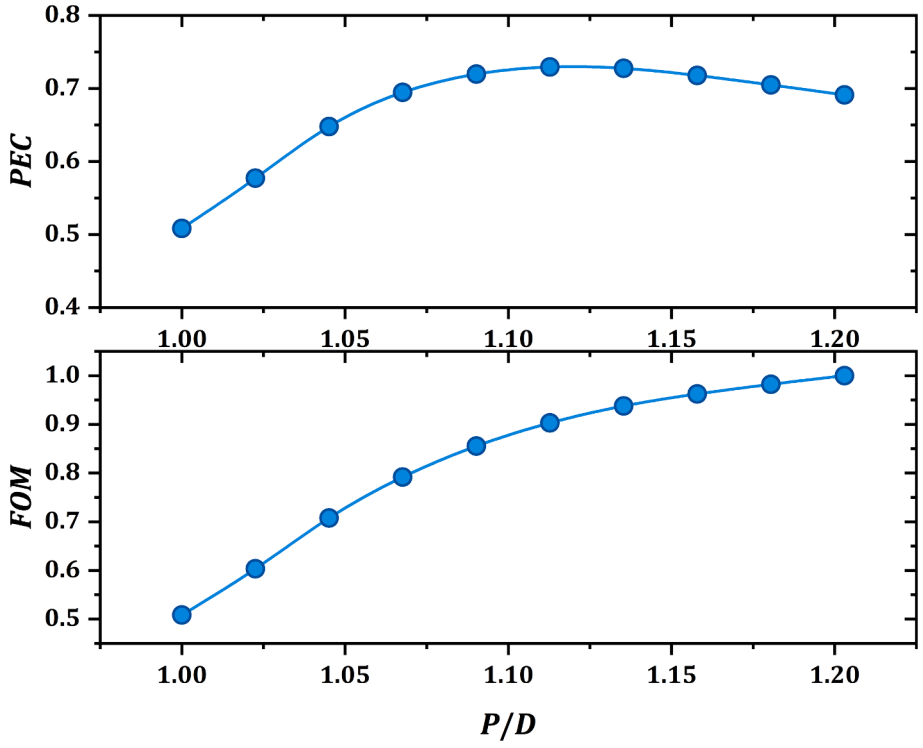

Fig. 18. Figure of merit and performance evaluation criteria for various P/D for $Re = 7853$.

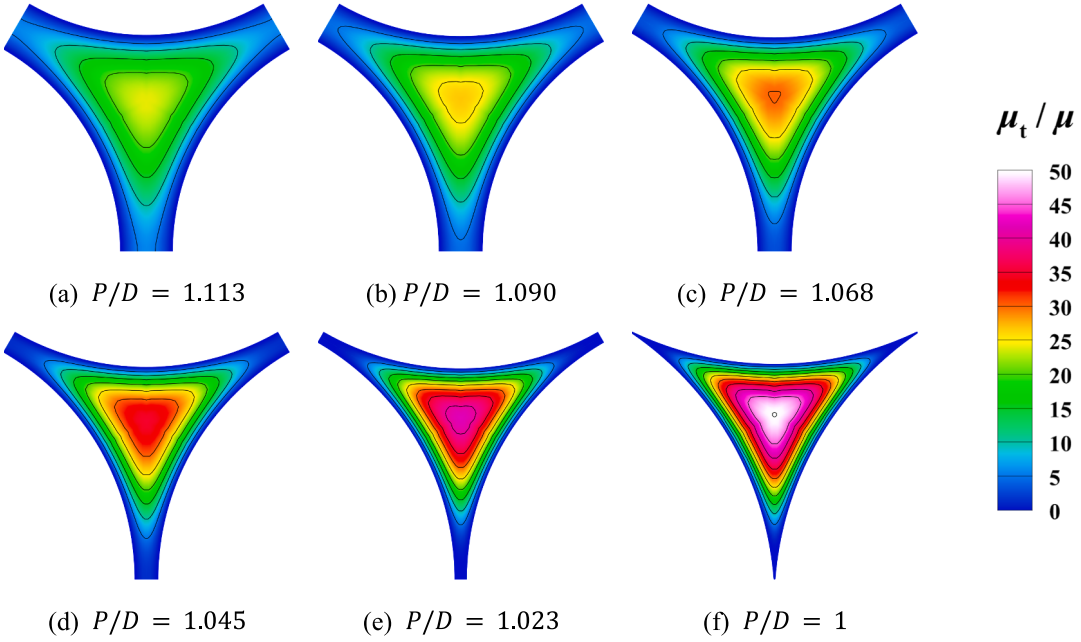

Fig. 19. Turbulent viscosity ratio contours at the effective heating distance of 400 mm for Re = 7853.

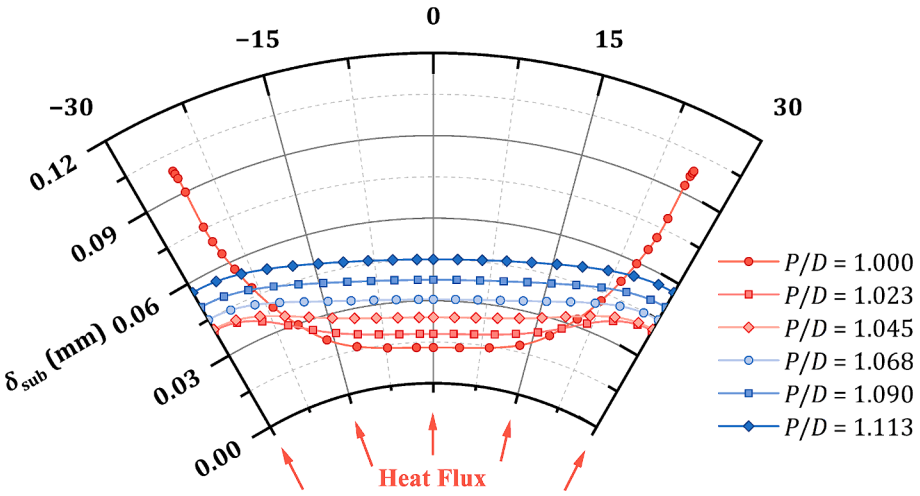

Fig. 20. Thickness of viscous sublayer at the effective heating length of 400 mm for Re = 7853.

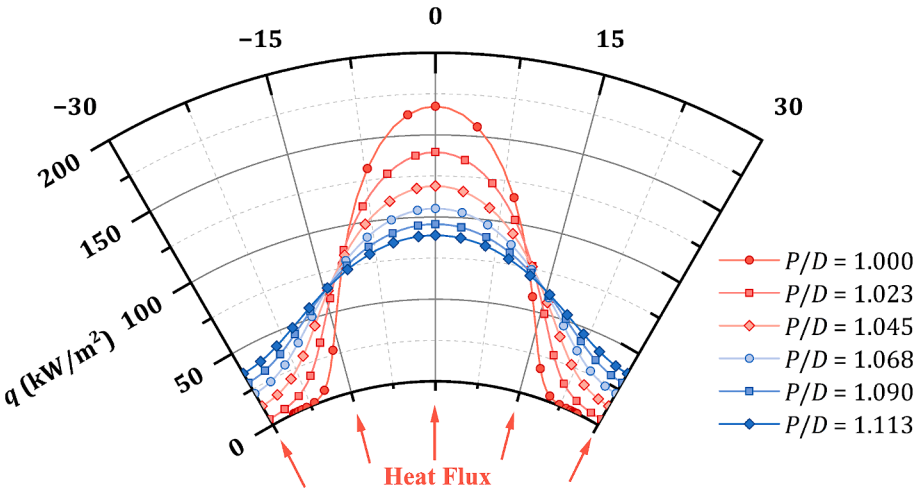

Fig. 21. Heat flux of cladding at the effective heating length of 400 mm for Re = 7853.

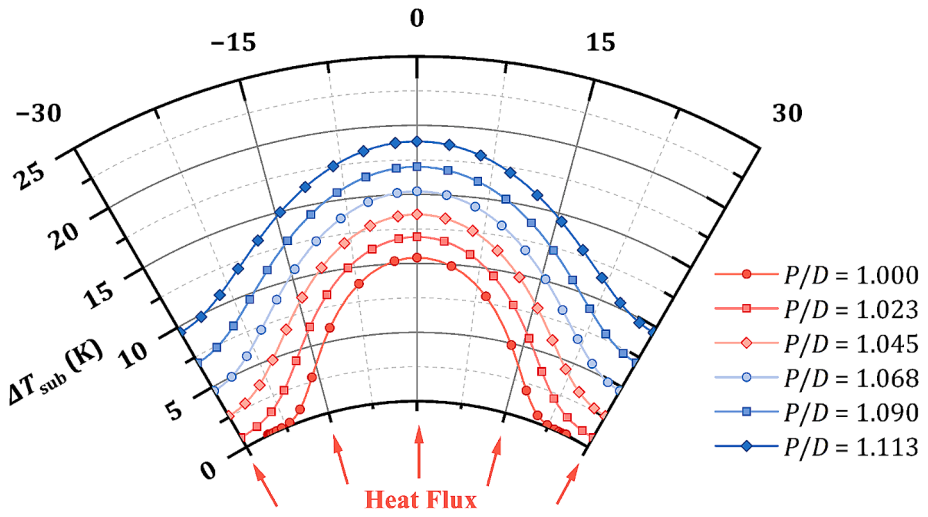

Fig. 22. Temperature difference of viscous sublayer at the effective heating length of 400 mm for $Re = 7853$.

coefficient without conjugate heat transfer is only 8.85 % of that with conjugate heat transfer in the quasi-triangular pipe. That is because the heat transfer at the slit is poor and the wall temperature reaches a peak without conjugate heat transfer. However, the heat conduction of the cladding redistributes the heat flux, increasing at $\theta = 0^{\circ}$ and decreasing at $\theta = 30^{\circ}$ and the heat flux redistribution flattens the wall temperature with conjugate heat transfer.

- The decrease in pitch-to-diameter ratio enhances the convective heat transfer of helium-xenon gas mixture and lowers the wall temperature of rod bundles for the same Reynolds number. When P/D decreases from 1.2 to 1, the heat transfer coefficient increases to 2.3 times. However, it also causes larger pressure drops. A new performance evaluation criterion (PEC) is presented considering the effects of heat transfer, pressure drop and volume. PEC first increases and then decreases with the increase in P/D. The results indicate the best comprehensive performance occurs at $P/D = 1.113$.
- The heat transfer mechanism of He-Xe in tight rod bundles is analyzed. Analysis shows that the decrease in P/D enhances the turbulent effect of He-Xe, reduces the thickness of viscous sublayer and decrease the thermal resistance of viscous sublayer, which is the main reason for the heat transfer enhancement.
- Considering the effects of P/D, empirical correlations of Nusselt number and friction factor for helium-xenon gas mixture in tight rod bundles were presented, which can be used for engineering design and optimization.

In the future, we hope to further investigate the effects of spacers and radiation heat transfer on the He-Xe heat transfer in tight rod bundles.

CRediT authorship contribution statement

Junren Hou: Writing – original draft, Visualization, Validation, Methodology, Investigation, Data curation. **Yuan Zhou:** Writing – review & editing, Supervision, Conceptualization. **Shanfang Huang:** Writing – review & editing, Conceptualization.

Declaration of competing interest

The authors declare that they have no known competing financial interests or personal relationships that could have appeared to influence the work reported in this paper.

Data availability

Data will be made available on request.

Acknowledgments

This work was supported by the National Natural Science Foundation of China [grant numbers U2241278]. The authors gratefully acknowledge the support of the funding agencies.

Appendix A. The effect of helium gap in heat transfer

Figure A1 shows the temperature distribution at $L = 400$ mm and $\theta = 0^{\circ}$ for $P/D = 1.113$ and $Re = 7853$. The results show that the helium gap has no effect on the temperature distribution in the cladding and coolant. However, it leads to an increase in the temperature of the fuel. In this study, the average thermal conductivity of Mo-Re is 64.74 W/(m·K). The average thermal conductivity of UO_2 is 3.104 W/(m·K). The average thermal conductivity of helium is 0.444 W/(m·K). Because the thermal conductivity of helium is much lower than that of the fuel and UO_2, the result shows that the gas gap has the effect of surface thermal resistance. When the gas gap is filled with UO_2 or Mo-Re the temperature distribution does not significantly jump in the gas gap. Since the low thermal conductivity of helium, when the gas gap is filled with helium, temperature jumps in the gas gap.

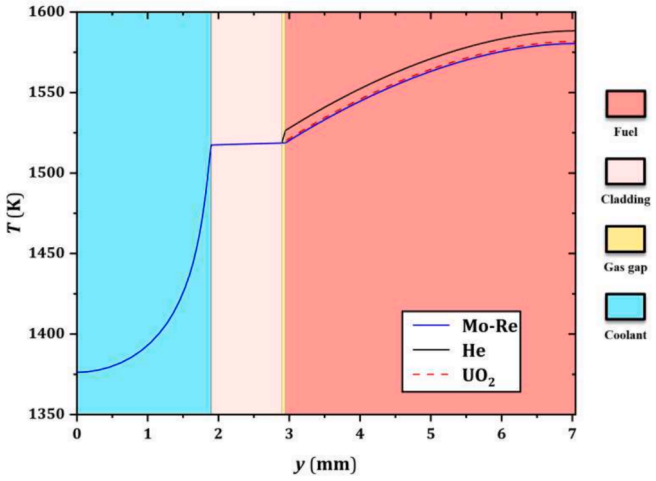

Fig. A1. Comparison of the influence of gas gap on heat transfer. The legend represents the material filled in the gas gap.

Since helium is monatomic molecules and have no ability to absorb and emit radiation, they can be regarded as transparent bodies of thermal radiation. Because the inner surface of gas gap is a convex surface, its heat flux brought by radiation can be calculated by Eq. (A1) and (A2):

$$q_i = \epsilon_s C_0 \left[\left(\frac{T_i}{100} \right)^4 - \left(\frac{T_o}{100} \right)^4 \right] \tag{A1}$$

$$\epsilon_s = \frac{1}{\frac{1}{\epsilon_i} + \frac{A_i}{A_o}\left(\frac{1}{\epsilon_o} - 1 \right)} \tag{A2}$$

where ϵ is emissivity, C_0 is blackbody radiation coefficient equal to 5.67 W/(m^2·K^4), A is the surface areas. The subscript i represents the inner surface and o represents the outer surface. The inner surface temperature of the gas gap is 1526.4 K. The outer surface temperature of the gas gap is 1518.6 K. The temperature difference between the two sides of gas gap is about 7.8 K. Assuming that the emissivity of both the inner and outer surfaces is 0.6, the calculated heat flux brought by radiation is 2682.5 W/m^2. Compared with Fig. 5(b), result shows that the heat flux brought by radiation is only about 4 % of the total heat flux. Radiative heat transfer can reduce the thermal resistance of the helium gap. From the analysis in the previous paragraph, it is known that a heat flux of 4 % is able to reduce the fuel temperature by about 0.3 K, with no effect on the temperature of cladding and coolant. Therefore, radiative heat transfer does have an effect, but it is not significant and is not considered in this paper. We hope to be able to study it in detail in subsequent work.

References

[1] A. Peakman, B. Lindley, A review of nuclear electric fission space reactor technologies for achieving high-power output and operating with HALEU fuel, Prog. Nucl. Energy. 163 (2023) 104815.

[2] Z. Liu, K. Cheng, Z. Yin, Z. Wang, J. Wang, J. Qin, Evaluation of the CBC-ORC energy system in lunar base: Working fluid combination selection, day and night operation performance, Energy Convers. Manage. 257 (2022) 115445.

[3] W. MJ, Z. MJ, Prometheus project reactor module final report, for naval reactors information, Knolls Atomic Power Lab. (2006).

[4] B. Levine, Space nuclear power plant pre-conceptual design report, for information, Knolls Atomic Power Lab.(KAPL), Niskayuna, NY (United States) (2006).

[5] R. Zhang, K. Guo, C. Wang, D. Zhang, W. Tian, S. Qiu, G. Su, J. Deng, Thermal-hydraulic analysis of gas-cooled space nuclear reactor power system with closed Brayton cycle, Int. J. Energy Res. 45 (8) (2021) 11851–11867.

[6] H. Qin, R. Zhang, K. Guo, C. Wang, W. Tian, G. Su, S. Qiu, Thermal-hydraulic analysis of an open-grid megawatt gas-cooled space nuclear reactor core, Int. J. Energy Res. 45 (8) (2021) 11616–11628.

[7] T. Meng, K. Cheng, F. Zhao, C. Xia, S. Tan, Computational flow and heat transfer design and analysis for 1/12 gas-cooled space nuclear reactor, Ann. Nucl. Energy. 135 (2020) 106986.

[8] T. Meng, F. Zhao, K. Cheng, C. Zeng, S. Tan, Neutronics analysis of megawatt-class gas-cooled space nuclear reactor design, J. Nucl. Sci. Technol. 56 (12) (2019) 1120–1129.

[9] C. Guan, X. Chai, T. Zhang, X. Liu, H. He, Mass and efficiency optimization of a He-Xe Brayton cycle for mobile, land-based nuclear microreactors, Energy Convers. Manage. 301 (2024) 118011.

[10] M.S. El-Genk, J.-M. Tournier, Noble-Gas Binary Mixtures for Closed-Brayton-Cycle Space Reactor Power Systems, J. Propul. Power. 23 (4) (2007) 863–873.

[11] J.-M.-P. Tournier, M.S. El-Genk, Properties of noble gases and binary mixtures for closed Brayton Cycle applications, Energy Convers. Manage. 49 (3) (2008) 469–492.

[12] M. Taylor, K. Bauer, D. McEligot, Internal forced convection to low-Prandtl-number gas mixtures, Int. J. Heat Mass Transf. 31 (1) (1988) 13–25.

[13] B. Zhou, H. Zhang, Y. Ji, J. Sun, Y. Sun, A. Serikov, Numerical investigation on turbulent flow and heat transfer of helium-xenon gas mixture in a circular tube, Sci. Technol. Nucl. Install. 2021 (2021) 1–12.

[14] B. Zhou, Y. Ji, J. Sun, Y.-L. Sun, Nusselt number correlation for turbulent heat transfer of helium–xenon gas mixtures, Nucl. Sci. Tech. 32 (11) (2021) 128.

[15] B. Zhou, Y. Ji, J. Sun, Y. Sun, Modified turbulent Prandtl number model for helium–xenon gas mixture with low Prandtl number, Nucl. Eng. Des. 366 (2020) 110738.

[16] H. Qin, C. Wang, W. Tian, S. Qiu, G. Su, Experimental investigation on flow and heat transfer characteristics of He-Xe gas mixture, Int. J. Heat Mass Transf. 192 (2022) 122942.

[17] T.-S. Wang, X. Chai, C.-R. Guan, X.-Y. Liu, J.-L. Deng, H. He, X.-J. Liu, Numerical and theoretical investigations of heat transfer characteristics in helium–xenon cooled microreactor core, Nucl. Sci. Tech. 34 (11) (2023) 1–19.

[18] V.E. Nakoryakov, O.V. Vitovsky, Study of heat transfer of a helium–xenon mixture in heated channels with different cross-sectional shapes, J. Appl. Mech. Tech. Phys. 58 (4) (2017) 664–669.

[19] O.V. Vitovsky, S.L. Elistratov, M.S. Makarov, V.E. Nakoryakov, V.S. Naumkin, Heat transfer in a flow of gas mixture with low Prandtl number in triangular channels, J. Eng. Thermophys. 25 (1) (2016) 15–23.

[20] V.E. Nakoryakov, S.L. Elistratov, O.V. Vitovsky, E.Y. Slesareva, Experimental investigation of heat transfer in helium-xenon mixtures in triangle channels, J. Eng. Thermophys. 24 (2) (2015) 139–142.

[21] S.L. Elistratov, O.V. Vitovskii, E.Y. Slesareva, Experimental investigation of heat transfer of helium-xenon mixtures in cylindrical channels, J. Eng. Thermophys. 24 (1) (2015) 33–35.

[22] O.V. Vitovsky, Experimental study of heat transfer during the flow of a gas coolant in a heated quasi-triangular channel, Int. J. Heat Mass Transf. 190 (2022) 122771.

[23] M.S. Makarov, O.V. Vitovsky, V.S. Naumkin, K.S. Lebeda, Investigation of hydraulic resistance and heat transfer in the flow of HE-XE mixture with a small

Prandtl number in a quasi-triangular pipe, Int. J. Heat Mass Transf. 199 (2022) 123427.
[24] H. Qin, Y. Fang, C. Wang, W. Tian, S. Qiu, G. Su, J. Deng, Numerical investigation on heat transfer characteristics of helium-xenon gas mixture, Int. J. Energy Res. 45 (8) (2020) 11745–11758.
[25] Q. Sun, H. Zhang, Numerical study on heat transfer performance of cooling channels in space core, Appl. Therm. Eng. 210 (2022) 118274.
[26] K. Ning, Y. He, F. Zhao, X. Dong, M. Gui, R. Sun, S. Tan, Numerical investigation on flow and heat transfer characteristics of helium–xenon gas mixture in rod bundles, Prog. Nucl. Energy. 166 (2023) 104947.
[27] C. Wang, S. Chen, W. Tian, G. Su, S. Qiu, Thermal-hydraulic analysis of He–Xe gas mixture in 2× 2 rod bundle wrapped with helical wires, Nucl. Eng. Technol. 55 (7) (2023) 2534–2546.
[28] O.V. Vitovsky, M.S. Makarov, V.E. Nakoryakov, V.S. Naumkin, Heat transfer in a small diameter tube at high Reynolds numbers, Int. J. Heat Mass Transf. 109 (2017) 997–1003.
[29] R. Zhang, T. Cong, G. Su, J. Wang, S. Qiu, Investigation on the critical heat flux in typical 5 by 5 rod bundle at conditions prototypical of PWR based on CFD methodology, Appl. Therm. Eng. 179 (2020) 115582.
[30] B.S. Shin, S.H. Chang, CHF experiment and CFD analysis in a 2×3 rod bundle with mixing vane, Nucl. Eng. Des. 239 (5) (2009) 899–912.
[31] T. Cong, R. Zhang, L. Chen, X. Zhang, T. Yu, Studies on the subcooled boiling in a fuel assembly with 5 by 5 rods using an improved wall boiling model, Ann. Nucl. Energy. 114 (2018) 413–426.
[32] A. Fluent, Ansys Fluent Theory Guide, Ansys Inc, USA, 2011, pp. 724–746.
[33] J. Hou, Y. Zhou, Y. Yuan, S. Huang, Numerical study on flow structure and heat transfer of supercritical CO2 in tubes with different inclination angles, Prog. Nucl. Energy. 168 (2024) 105028.
[34] F.R. Menter, Two-equation eddy-viscosity turbulence models for engineering applications, AIAA Journal. 32 (8) (1994) 1598–1605.
[35] J. Hou, Q. Song, H. Leng, C. Xue, Y. Yuan, Y. Zhou, A non-destructive model for thermal-hydraulics of wire-wrapped rod bundle and wire-rod contact corner microscopic behavior, Prog. Nucl. Energy. 154 (2022) 104469.
[36] S. Popov, J.J. Carbajo, G. Yoder, Thermophysical properties of MOX and UO2 fuels including the effects of irradiation, ORNL. 27 (2000), 4-00.
[37] E.W. Lemmon, M.L. Huber, M.O. McLinden, NIST reference fluid thermodynamic and transport properties–REFPROP, NIST Standard Reference Database. 23 (2002) v7.
[38] L. Lundberg, Critical evaluation of molybdenum and its alloys for use in space reactor core heat pipes, Los Alamos National Lab.(LANL), Los Alamos, NM (United States) (1981).
[39] J.-M. Tournier, M. El-Genk, B. Gallo, Best estimates of binary gas mixtures properties for closed Brayton cycle space applications, in: 4th International Energy Conversion Engineering Conference and Exhibit (IECEC), 2006, p. 4154.
[40] F.W. Dittus, Heat transfer in automobile radiators of the tubular type, Univ. of California Pub., Eng. 2 (13) (1930) 443–461.
[41] W.M. Kays, M.E. Crawford, B. Weigand, Convective heat and mass transfer, McGraw-Hill New York, 1980.
[42] H. Blasius, Das aehnlichkeitsgesetz bei reibungsvorgängen in flüssigkeiten, in: Mitteilungen Über Forschungsarbeiten Auf Dem Gebiete Des Ingenieurwesens: Insbesondere Aus Den Laboratorien Der Technischen Hochschulen, Springer, 1913, pp. 1–41.
[43] R.L. Webb, Performance evaluation criteria for use of enhanced heat transfer surfaces in heat exchanger design, Int. J. Heat Mass Transf. 24 (4) (1981) 715–726.
[44] M.H. Tusar, P.K. Bhowmik, B. Salam, J. Uddin Ahamed, J.K. Kim, Convective heat transfer and friction factor characteristics of helical strip inserted annuli at turbulent flow, Int. J. Heat Mass Transf. 176 (2021) 121422.
[45] M. Pourramezan, H. Ajam, Modeling for thermal augmentation of turbulent flow in a circular tube fitted with twisted conical strip inserts, Appl. Therm. Eng. 105 (2016) 509–518.
[46] G. Tang, H. Shi, Y. Wu, J. Lu, Z. Li, Q. Liu, H. Zhang, A variable turbulent Prandtl number model for simulating supercritical pressure CO2 heat transfer, Int. J. Heat Mass Transf. 102 (2016) 1082–1092.
[47] H. Eckelmann, The structure of the viscous sublayer and the adjacent wall region in a turbulent channel flow, J. Fluid Mech. 65 (3) (1974) 439–459.